Accepted Manuscript

Thermal behaviour and fungi resistance of composites based on wood and natural and synthetic epoxy resins cured with maleopimaric acid

Liliana Rosu, Fanica Mustata, Cristian–Dragos Varganici, Dan Rosu, Teodora Rusu, Irina Rosca

PII: S0141-3910(18)30408-7

DOI: https://doi.org/10.1016/j.polymdegradstab.2018.12.022

Reference: PDST 8730

To appear in: *Polymer Degradation and Stability*

Received Date: 15 October 2018

Revised Date: 6 December 2018

Accepted Date: 16 December 2018

Please cite this article as: Rosu L, Mustata F, Varganici Cristian–Dragos, Rosu D, Rusu T, Rosca I, Thermal behaviour and fungi resistance of composites based on wood and natural and synthetic epoxy resins cured with maleopimaric acid, *Polymer Degradation and Stability* (2019), doi: https://doi.org/10.1016/j.polymdegradstab.2018.12.022.

Thermal behaviour and fungi resistance of composites based on wood and natural and synthetic epoxy resins cured with maleopimaric acid

Liliana Rosu[a], Fanica Mustata[b], Cristian–Dragos Varganici[a*], Dan Rosu[a], Teodora Rusu[a], Irina Rosca[a]

[a]*Centre of Advanced Research in Bionanoconjugates and Biopolymers, "Petru Poni" Institute of Macromolecular Chemistry, 41A Gr. Ghica-Voda Alley, 700487 Iasi, Romania*

[b]*"Petru Poni" Institute of Macromolecular Chemistry, 41A Gr. Ghica–Voda Alley, 700487 Iasi, Romania*

Abstract

Wood/epoxy resin composites based on diglycidyl ether of bisphenol A (DGEBA)/epoxidized oil (EO)/Diels–Alder adducts of resin acids with maleic anhydride (RAMA) in acetone (80 %) were obtained by impregnation. Epoxidation was carried out in the presence of hydrogen peroxide (H_2O_2), acetic acid (AAc), sulfuric acid (H_2SO_4) as catalyst and cyclohexane (CHx) as solvent at a molar ratio of 0.5/1.5/1 (AAc/hydrogen peroxide/ethylene unsaturation). The kinetic parameters (activation energy and pre–exponential factor) of the DGEBA/EO/RAMA curing reaction and thermal characterization of the crosslinked compounds and wood epoxy composites (WECs) were obtained using differential scanning calorimetry (DSC) and thermogravimetric analysis (TGA). Based on the chemical structure of the evolved gases resulted during thermal decomposition of the crosslinked polymers and WECs, identified with FT–IR, a probable mechanism of thermal degradation was proposed. Resistance to three fungi was also tested.

Keywords: Wood, Thermosetting resin, Cure behaviour, Thermal properties, Biological resistance

[*]To whom correspondence should be adressed:
Phone: +40 232 217 454
Fax: +40 232 211 299
E-mail address: varganici.cristian@icmpp.ro

1. Introduction

Nowadays, composites based on natural materials are widely used in industrial and household fields, because they are environmentally friendly and originate from renewable resources. Wood is among the most important renewable resources. It has a great importance for life sustainability, as well as both raw and processed material. The most important components of wood are lignin, cellulose, hemicelluloses and resins. Under environmental factors influence (i.e. temperature, light, moisture, microorganisms, insects, etc.), there occurs wood damage, followed by a decrease in technical (thermal, mechanical and electrical behaviour) and aesthetic aspects [1, 2].

To preserve the properties of wood, physical and chemical methods, including heat treatment, chemical modification, impregnation and physical coatings, have been used. Considering its chemical structure (mainly hydroxyl groups), wood was modified by esterification and etherification reactions with anhydrides, acids, acid chlorides, epoxy resins, unsaturated derivatives, cyclic ethers, lactones, alkyl chlorides and so on. These transformations were aimed to improve mechanical and electrical properties, as well as to enhance resistance to environmental factors action [3–13].

Vegetable oils (edible or non–edible) are a renewable source of raw materials, mainly esters of glycerol, which are the result of glycerol esterification with three saturated and/or unsaturated fatty acids [14]. As a consequence of the chemical structures, these oils may be modified to obtain new monomers that can induce special properties in the final polymers (flexibility, biocompatibility, biodegradability, thermal stability) [4, 15–20]. Hemp oil and flax oil, as non–edible oils that contain a large number of unsaturated groups in their structure, represent an excellent source of raw material for the synthesis of monomers with new functional groups capable to polymerize. One of the most common methods of chemical modification of vegetable oils is epoxidation. Epoxidized oils may be used as basis for their transformation in acrylated, methacrylated, hydroxylated monomers, used either individually or mixed in various polymeric compositions [16, 17, 21–25]. Also, vegetable oils and their derivatives, alone or in combination with various fungicides, have been used to increase the decay resistance of wood [26, 27].

Rosin is a renewable naturally raw material consisting of neutral compounds (turpentine) and resin acids (abietic, levopimaric, neoabietic, palustric, fatty acids, etc.). As a consequence of their chemical structure, the resin acids can be converted into several types of monomers. In particular, the most common transformation is the Diels–Alder reaction, when some polyacids are obtained and further used as

crosslinking agents for epoxy resins [28–35]. These adducts, through their chemical structure, may improve the properties of the crosslinked epoxy resins.

Epoxy resins are some of the most widely available synthetic monomers, which, after curing, present excellent electrical, mechanical and thermal properties in a vast palette of application fields, although not being environmentally friendly [36, 37]. This behaviour depends on the formulation, chemical composition and crosslinking conditions. By using some natural ingredients (rosin acids and vegetable oil derivatives), these formulations may compensate some drawbacks and be environmentally friendly [16, 20, 28–35, 38, 39].

The paper describes the curing and non–isothermal degradation kinetics of compositions based on DGEBA/EO/RAMA and WECs. The novelty of the work consists in the using of some epoxy resins based on vegetable oils and of a curing agent derived from resinic acids of natural origin. Also, the thermal and fungal resistance properties were followed using DSC and TG analyses. Based on FT–IR analysis of the evolved gases during thermal decomposition a possible degradation mechanism is proposed.

2. Experimental

2.1. Materials

Hydrogen peroxide (H_2O_2), glacial acetic acid (AAc), maleic anhydride (MA), potassium hydroxide (KOH), sulfuric acid (H_2SO_4), triethylbenzylammonium chloride (TEBAC) and anhydrous sodium sulfate (Na_2SO_4) were analytical grade products and used without any purification. The solvents were used as received or distilled before use. Resin acids (RA) were obtained from commercial rosin by acid isomerization and by repeated recrystallizations from concentrated acetone solutions and had an acid number (a. n.) of 181 mg KOH g^{-1} and melting point (m. p.) of 161 ^oC [33]. RAMA with m. p. 230 ^oC and a. n. 434 mg KOH g^{-1} was obtained following a procedure described in the literature [40]. DGEBA, a commercial product (Sintofarm, Romania), (average epoxy equivalent weight of 190 g eq^{-1}, viscosity of 12000 mPas at 25 °C) was used as received. Flax oil (FO) and hemp oil (HO) have been obtained from the local market and have the following compositions supplied by the manufacturers: flax oil [saturated fats 10.1 wt. %, unsaturated fats (oleic acid 22.4 wt. %, linoleic acid 14.3 wt. %, α–linolenic acid 52.3 wt. %), other acids 0.9 wt. %] and hemp oil [saturated fats 8 wt. %, unsaturated fats (oleic acid 11.4 wt. %, linoleic acid 57 wt. %, α–linolenic acid 18.7 wt. %, other acids 2.9 wt. %)]. Epoxidized flax oil (EFO) (number of epoxy groups 5.9 mol^{-1}) was obtained as described below and epoxidized hemp oil (EHO) (number of epoxy group 3.5 mol^{-1})

was obtained following a procedure described in the literature [23]. The number of epoxy groups was measured using ^{1}H–NMR spectroscopy. The softwood samples (W) (*Abies alba L.*) had the same characteristics as those presented in a previous work [9].

2.2. Sample preparation for DSC and TGA studies

For the DSC studies, the formulation DGEBA/EO/RAMA at a molar ratio of 0.8/0.2/0.66 (epoxy ring/carboxyl proton 1/1) in the presence of TEBAC as catalyst was prepared. After a vigorous mixing of the reactants, they were degassed in a vacuum oven at room temperature and a portion has been stored at 0 °C before the DSC recording was performed. The DGEBA/EO/RAMA compositions used for the TG characterization were transferred in an aluminum form and crosslinked according to the following protocol: 1 h at 100 ^{o}C, 1 h at 135 ^{o}C and post cured 4 h at 185 ^{o}C (Scheme 1).

Scheme 1

The WEC samples were obtained by immersion of W samples for 8 h in the next formulation: DGEBA/EO/RAMA at molar ratio 0.8/0.2/0.66, 80 wt. % solution in acetone, in the presence of TEBAC as catalyst. After immersion, the impregnated samples were placed in a vacuum oven at 40 ^{o}C and maintained another 8 h to release the solvent. Then, the WECs were cured at 70 ^{o}C for 1 h, 1 h at 100 ^{o}C, 1 h at 135 ^{o}C and then post cured at 150 ^{o}C for 3 h and used for TGA studies. The same samples were also used for crystallinity measurements and for morphological analysis. The weight fraction of W in WECs was 90 %.

2.3. Measurements and methods

The acid number (a.n.) was obtained using a slightly modified ASTM D 465–05. The sample dissolved in acetone at 10 % (w/v) concentration was titrated with 0.5 N ethanolic KOH solutions in the presence of phenolphthalein as indicator [35, 41]. The epoxy equivalent weights (EEW) were obtained using ASTM D 1652–04 [42]. The number of the double bonds from oils was obtained using ^{1}H–NMR spectroscopy, with the next equation [43]:

$$D_b = 0.5(A - N_f) / N_f \quad (1)$$

where: D_b is the double bonds number, A is the surface assigned to the olefinic protons located between 5.2 and 5.4 ppm and N_f is the normalization factor (obtained through the dividing by 4 of the protons area from 4.0 and 4.3 ppm assigned to terminal protons of glycerol).

The melting points were obtained with a DSC 200 F3 Maia device (Netzsch, Germany), at 10 ^{o}C min^{-1} heating rate.

FT-IR spectra were acquired with a Vertex 70 apparatus (Bruker–Germany) using KBr pellets. ^{1}H–NMR spectra of DGEBA, oils, epoxidized oils and RAMA were recorded with an Avance DRX 400 (Bruker–Germany) apparatus at 50 ^{o}C using $CDCl_3$ and DMSO–d_6 as solvents and tetramethylsilane (TMS) as internal standard.

TG curves were recorded in the temperature range 30–600 ^{o}C, in inert atmosphere (N_2 flow rate of 40 mL min^{-1}) at three heating rates (10, 20 and 30 ^{o}C min^{-1}) using STA 449 F1 Jupiter device (Netzsch–Germany). Open Al_2O_3 crucibles were loaded with approximately 10 mg of the ground sample. Gaseous products resulting from thermal degradation were transferred through a transferring line made from Teflon, coupled to the head of the TG balance, with 1 m length and with 1.5 mm diameter (heated at 190 ^{o}C to limit condensation) to the FTIR apparatus having a MCT detector (Mercury Cadmium Telluride). The FT–IR spectra were recorded between 4000 and 500 cm^{-1} wavenumber values and processed with OPUS 6.5 software.

DSC analysis was undertaken on a DSC 200 F3 Maia apparatus (Netzsch, Germany), under nitrogen flow rate of 50 mL min^{-1}, at three heating rates (5, 10 and 15 ^{o}C min^{-1}) in the temperature range 25–300 ^{o}C. The calibration of the apparatus was made with high purity indium. The samples weighing up to 10 mg were placed in aluminum cells provided with a pierced lid, were scanned in the presence of one aluminum empty cell as standard. The heat flow versus temperature was recorded. DSC data were recorded consecutively using the same sample on the same day [44].

The evaluation of the kinetic parameters, both for curing and thermal degradation reactions were obtained using DSC and TG scans and processed with Netzsch Thermokinetics 3 software [45]. In a first instance, these parameters were evaluated on the basis of free–estimation methods of Ozawa–Flynn–Wall (OFW) and Friedman (FD). The used equations are as follows [46–48].

$$\ln\beta = C - 1.052(E_O/RT_p) \qquad \text{(OFW equation)} \qquad (2)$$

and

$$\ln\left(\frac{d\alpha}{dT}\right) = \ln\left(\frac{A}{\beta}\right) + \ln(f(\alpha)) - \frac{E_{FD}}{RT} \qquad \text{(FD equation)} \qquad (3)$$

where: A is the frequency factor, β is the heating rate, C is a constant, E_O and E_{FD} are the specific activation energies of reactions obtained with OFW and FD relations, T_p is the exothermic peak temperature in Kelvin and R is universal gas constant.

These methods, included in "Netzsch Thermokinetics 3", a software module for the kinetic analysis of thermal measurements, permit the evaluation of the kinetic parameters and the variation of activation energy values versus conversion degree, without assuming any reaction model. Changes in the shape of the activation energy versus the degree of conversion curves indicate that the degradation reactions occur following a complex mechanism in several independent stages through consecutive, parallel or competitive processes [49, 50]. This makes it possible to choose between different mechanisms and obtain a global model that gives the best results for the curing or thermal degradation processes.

Morphological study of WECs was conducted by analyzing the scanning electron microscopy (SEM) images. These were obtained using the SEM/ESEM–EDAX–QUANTA 200 apparatus which operated in the following parameters: field emission filament 16 kV accelerating voltage, high vacum mode and maximum magnification of 5000 X. The images were obtained on the surface samples, cut perpendicularly on the sense of growth and gilded to make them conductive.

Anti–decay resistance testing was performed on untreated wood (blank), polymer and WECs. The test samples were obtained as previously described above. The main components of wood (cellulose, hemicelluloses, lignin), under favorable conditions of humidity and temperature, can be metabolized by fungi as nutrients, resulting in wood degradation. Four samples from each specimen, dried to constant weight at 105 ^{o}C, were tested in the same conditions for resistance against decay. The following fungi were used: a white rot fungus *Penicillium chrysogenum* ATCC10106 (*P. chrysogenum*), a brown rot fungus *Cladosporium cladosporioides* ATCC16022 (*C. cladosporioides*) and black rot fungus *Aspergillus brasiliensis* ATCC 9642 (*A. brasiliensis*). The samples were placed in Petri dishes on a substrate of malt extract (for *P. chrysogenum*) and potato dextrose (for *C. cladosporioides* and *A. brasiliensis*) in agar which were previously inoculated with a standard inoculum of 0.5 McFerland for each fungal strain. All the Petri dishes were incubated at the room temperature (24 ± 1 °C) for 10 weeks. The fungal growth on the untreated and treated samples was monitored during the 10 weeks of incubation and at the end of the experiment the wood samples were removed from the culture plates and the fungal biomass was gently removed with the aid of a wet cotton fabric. The wet samples were oven–dried at 105 ^{o}C, in order to reach constant weight. Then all the samples were accurately weighed in order to notice the retained moisture.

Crystallinity of W and WECs was measured with the aid of wide angle X–ray diffractometry (WAXD).The WAXD curves were recorded using a Bruker D8 Advance (Germany) apparatus with CuK_α monochromatic radiation (λ = 0.15406 nm) at 25 °C, 36 kV and 25 mA, in the interval 2θ diffraction angles (Bragg angle) ranging between 4 and 40 °.

The crystallinity index was calculated using the next equation [51]:

$$I_c\ (\%) = [(I_{002} - I_{am})/I_{002}] \cdot 100 \quad (4)$$

where: I_c is crystallinity index, I_{002} is maximum value of intensity at the 002 crystalline peak, I_{am} is the maximum value of amorphous peak intensity [52].

The polymer weight percentage gain (WPG) after crosslinking was calculated with the next equation:

$$WPG\ (\%) = [(M_f - M_i)/M_f] \cdot 100 \quad (5)$$

where: M_i is the initial weight of W and M_f is the final weight of WEC sample after crosslinking.

The humidity values after fungal attack were calculated as follows:

$$H\ (\%) = [(M_w - M_d)/M_w] \cdot 100 \quad (6)$$

where: H is the percent of the humidity; M_w is the weight of wet sample after fungal attack and M_d is the weight of the same sample after drying.

The weight losses (WL) (%), after the fungus attack were calculated with the equation:

$$WL\ (\%) = [(M_i - M_d)/M_i] \cdot 100 \quad (7)$$

where : M_i is the weight of initial sample before fungal attack and M_d is the weight of the same dried sample after fungal attack.

Twenty two solvents with solubility parameters (δ) between 7.24 up to 23.5 cal cm^{-3} were used to obtain the swelling parameter of the crosslinked polymers (Table 1). Each solvent used in the study was introduced in Erlenmeyer flasks equipped with plunger stoppers. Over each solvent, polymer samples with a weight of up to 0.1 g were added, maintaining the constant temperature (25 °C) for a long period of time. The weight of the swollen samples was measured until it was stabilized. The swelling degree was calculated with the following equation [53]:

$$Q\ (\%) = [(M_w - M_i)/M_i] \cdot 100 \quad (8)$$

where: Q is the swelling coefficient, M_w is the weight of the swollen sample and M_i is the weight of the initial sample.

Table 1

Fig. 1_revised

The solubility parameter of the crosslinked samples is obtained by observing the maximum of the swelling coefficient (Q) in the Q versus δ plot (Fig.1). As it may be seen from Fig. 1, the maximum value is reached for methylene chloride, which is the solvent that induces the highest degree of network swelling. It can be considered that the solubility parameter of methylene chloride, of 9.93 (cal cm^{-3})$^{0.5}$, may be attributed to the polymer–solvent interaction parameter of the crosslinked polymers. The molecular weight between two crosslinking points (Mc) and the crosslinking density (n) of DGEBA/EO/RAMA samples were obtained based on the swelling measurements and calculated with Flory–Rehner equation [54]:

$$n = -[\ln(1-V)+V+\chi \bullet V^2]/V_{mol}[V^{0.33}-V/2] \quad (9)$$

where: V is the volume fraction of polymer in swollen polymer, V_{mol} is the molar volume of the solvent and χ is the Flory solvent–polymer interaction parameter. The interaction parameter may be obtained with the equation:

$$\chi = \frac{V}{RT}(\delta_p - \delta_s)^2 \quad (10)$$

where: R is the gas constant, T is temperature in Kelvin, V is the molar volume of the solvent, δ_p is solubility parameter of polymer and δ_s is solubility parameter of solvent.

3. Results and discussion

3.1. Synthesis and characterization of epoxidized flax oil (EFO)

Into a 0.5 L four–necked reaction vessel placed in a water bath, equipped with mechanical stirrer, thermometer, a water reflux condenser and dropping funnel, 150 g FO, 120 g AAc, 2 mL H_2SO_4 (diluted in 4 mL of distilled water) and 40 mL CHx were introduced. CHx was used to reduce the viscosity of the mixture and to minimize the epoxy cycle opening. The reaction mixture was moderately stirred for about 30 minutes, purged with a slow flow of nitrogen and the water bath was cooled with ice to 10 °C. After 1 h, 220 g H_2O_2 30 % (w/w) was added in small portions under vigorous stirring, while maintaining the reaction mixture temperature at about 15 °C. After adding the entire amount of H_2O_2, the temperature of the reaction mixture was slowly raised to 55 °C and maintained at this level for another 6 h. For finishing the reaction, the mixture was heated to 65 °C for another 0.5 h and then cooled rapidly on ice water bath. The reaction mass was washed twice with distilled water at 35 °C and then with a 5 wt. % potassium carbonate solution until complete neutralization. Then, the water layer was discharged and EFO was kept on anhydrous sodium

sulfate to remove traces of water. Sodium sulfate was removed by filtration and CHx was removed at 60 °C in a rotary evaporator under vacuum. The final product was introduced in a polyethylene vessel and stored in the dark at 20 °C (Scheme 2).

Scheme 2

The obtained EFO was a low viscosity yellowish color liquid. Its chemical structure was confirmed using FT–IR and ^{1}H–NMR spectroscopy analysis. Since there are no significant differences between the FT–IR spectra of the two oils, only the spectra of flax oil and epoxidized flax oil are shown in Fig. 2. The main signals are: 3470 cm^{-1} (OH stretching from opened epoxy ring), 2921 and 2859 cm^{-1} (CH_3, CH_2, CH stretching vibrations from fatty acids moieties), 1742 cm^{-1} (CO stretching in ester groups), 1455 cm^{-1} (CH aliphatic), 1242 and 1157 cm^{-1} (C–O–C ester linkages) and 823 cm^{-1} (oxirane rings). The signals from 3010 cm^{-1} and 1654 cm^{-1} from FO (specific to the olefin double bond) disappear and a new signal appears at 823 cm^{-1} specific to the epoxide groups from epoxidized oils (Fig. 2b). ^{1}H–NMR spectra of FO and EFO are presented in Fig. 3. The main signals are: 5.182 (the proton located at the secondary C of glycerol), 4.130 - 4.290 (glycerol protons), 2.805 - 3.091 (epoxy group protons), 2.28 (methylene protons adjacent to ester groups), 1.25 - 1.47 (methylene protons); 0.85 - 0.92 (methyl protons). The main difference which appears between the ^{1}H–NMR spectra of FO and EFO is the absence of the olefinic protons located near 5.35 ppm and presence of the protons attached to the epoxy ring with the peaks located at 2.770 and 3.091 ppm chemical shift.

Fig. 2_revised

Fig. 3_revised

3.2. FT–IR characterization of crosslinked polymers and WECs

In Fig. 4 there are presented the FT–IR spectra of W, crosslinked DGEBA/EFO/RAMA and WECs. As it may be observed in the DGEBA/EFO/RAMA and WECs spectra, they do not show any signal specific to the epoxy rings (at 915 cm^{-1} for DGEBA and at 823 cm^{-1} for EFO), confirming the reaction between the epoxy and carboxyl groups from RAMA. As a result of this reaction, a number of new hydroxyl groups are generated. Their corresponding signals are located at 3346 cm^{-1} in the WEC spectrum (Fig. 4c) and overlap with the signal from 3343 cm^{-1} specific to wood (Fig. 4a). Also, due to the above reaction, new ester groups appear, which are highlighted by the signal at 1724 cm^{-1} (C=O stretching vibrations) and signals from 1234 cm^{-1} and 1028 cm^{-1} (C–O–C stretching vibrations) (Figs 4b and 4c). There may also be observed a series of

signals located near 1606 and 1509 cm^{-1}, specific to skeletal vibrations of aromatic entities from DGEBA (Figs 4b and 4c).

Fig. 4_revised

3.3. Crosslinking density measurements

The crosslinking density (n) and the molecular weight between two crosslinking points (Mc) of DGEBA/EO/RAMA networks were determined using swelling measurements and a method described in the literature [54]. Based on the data from Fig. 1, the solubility parameter of methylene chloride [9.93 (cal cm^{-3}) $^{0.5}$] can be assigned as the polymer–solvent interaction parameter of the two crosslinked polymers. The following values were obtained: n = 2.065 10^{-3} mol cm^{-3} and Mc = 591 g mol^{-1} for DGEBA/EHO/RAMA sample and n = 1.862 10^{-3} mol cm^{-3} and Mc = 633 g mol^{-1} for DGEBA/EFO/RAMA. These values of Mc are quite close to the theoretical ones, suggesting a random distribution of the epoxidized oil molecules in the crosslinked polymer structure. The lowest value of Mc for DGEBA/EHO/RAMA sample is due to the smaller number of epoxy groups from EHO, fact which leads to a smaller degree of network packaging. The obtained networks have relative low T_g values (31 ^oC for DGEBA/EHO/RAMA and 32 ^oC for DGEBA/EFO/RAMA), as a consequence of internal plasticizing effect introduced by epoxy oils.

3.4. Curing of DGEBA/EO with RAMA

The obtained DGEBA/EO/RAMA samples (epoxy ring/carboxyl proton 1/1) were crosslinked in the DSC device at three heating rates. In Scheme 1 the chemical reactions between carboxyl and the epoxy groups from DGEBA/EO/RAMA are presented. Since the main reagents in these formulations have more than two reactive groups, with time and temperature increase, three–dimensional networks were obtained. As one may see from Fig. 5a (DSC curves for DGEBA/EFO/RAMA), with the increase in temperature, besides the main peak, a smaller sized peak appears, suggesting that few of the EFO epoxy groups (which have 6 epoxy groups) are partially sterically hindered, these groups further reacting with temperature increase. In the case of DGEBA/EHO/RAMA (Fig. 5b), the DSC curves show the same trend at 5 ^oC min^{-1}, while the records at high speeds, present only an exothermic peak, suggesting that all chemical reactions occur simultaneously. The evaluation of the kinetic parameters of the crosslinking reactions (apparent activation energy and preexponential factor) of the above samples was undertaken using the Friedman (FD) and Ozawa (OZ) methods [45–48].

Fig. 5_revised

If the curves shapes of apparent activation energy as a function of conversion factor show deviations from linearity, this fact suggests that the crosslinking takes place in several steps (maybe consist of a series of successive or parallel processes) and occur following a complex mechanism [49, 50]. From Figs. 6a and b, it may be observed that the apparent activation energy curves present few maximum and minimum values and depend on the chemical composition of the samples. This suggests that in order to establish the mechanism of the crosslinking process it is necessary for the evaluation to be done using the non–linear regression method (MLR) within the "Thermokinetics 3" software. Based on the initial values of the kinetic parameters obtained with the FD method and the shape of the DSC curves recorded at three heating rates, the software solves numerically the differential equations specific to 18 reaction types, adjusting the theoretical models to registered data. Following the processing of data by the software in the 0.1 to 0.9 conversion degree (α) interval, a three step kinetic model with successive reactions for the DGEBA/EFO/RAMA sample and a two steps model with successive reactions for the DGEBA/EHO/RAMA sample were chosen. The choice of these models was made using the difference between measured and calculated values, on the basis of the F–test and the best correlation coefficient between data.

The next conversion functions were used:

– n^{th} reaction order of the autocatalytic model, Cn:

$$f(\alpha) = (1-\alpha)^n (1+K_{cat}\cdot\alpha) \quad (11)$$

where: K_{cat} is the autocatalytic constant, *n* is the reaction order

– reaction order model, Fn:

$$f(\alpha) = (1 - \alpha)^n \quad (12)$$

where *n* is the reaction order and α is the conversion degree,

and

– Avrami–Erofeev reaction model, An:

$$f(\alpha) = n(1-\alpha)[-\ln(1-\alpha)]^{\frac{n-1}{n}} \quad (13)$$

where *n* is a constant parameter.

The following mechanisms of curing reactions were used:

– mechanism coded t:f,f; CnB,Fn,An; for formal kinetic model of A-1 $\rightarrow$ B-2 $\rightarrow$ C-3 $\rightarrow$ D type for DGEBA/EFO/RAMA

and

– mechanism coded d:f; CnB,Fn; for formal kinetic model of A-1 → B-2 → C type for DGEBA/EHO/RAMA

where: for DGEBA/EFO/RAMA sample, A is the initial reactant; B and C are the intermediate products and D is the final crosslinked resin,

and for DGEBA/EHO/RAMA sample, A is the initial reactant; B is the intermediate product and C is the final crosslinked resin.

The above codes are specific to "Thermokinetics 3" software (d:f; and t:f,f; represent reaction codes in two or three successive steps, while 1, 2, 3 denote the code for reaction steps). The results obtained from the above samples are showed in Table S1 (See Supporting Information). Using the data from Table S1 and the software, the DSC curves were recalculated. It can be seen that in the temperature range for which the calculations were performed, there is a good correlation between the experimental and the calculated data, which suggests that the proposed crosslinking mechanisms approximate well the real phenomenon. By comparing the data in Table S1, it can be seen that the values of the activation energies for DGEBA/EFO/RAMA are somewhat lower than those for DGEBA/EHO/RAMA. This fact can be explained on the basis of the different chemical structures of the two epoxy oils, EFO having several more epoxy groups than EHO, so the crosslinking reactions occur more easily.

Fig. 6_revised

3.5. Thermal degradation of the cured products and WECs

The chemical structure of the crosslinked polymers are presented in Scheme 1. In Fig. 7a there are given the TG and DTA curves of DGEBA/EFO/RAMA, obtained at three heating rates in nitrogen atmosphere. From Fig. 7a, the main degradation parameters ($T_{onset,}$ T_{peak}, T_{10}, T_{20}, T_{50} and W_{600}) are extracted and summarized in Table 2. Thermograms are very similar for both samples and the thermal parameters also. It can be noted that both polymers exhibit good thermal stability, mass losses being insignificant up to 350 ^{o}C. The kinetic parameters of the thermal degradation reaction (apparent activation energy and pre–exponential factor) were obtained using MLR. As it can be seen from Fig. 7b, the variation of the activation energy versus the conversion function degree presents a few minima and maxima, which suggests that the thermal degradation process occurs in at least two degradation steps [49, 50].

In a range of 0.1 to 0.9 of conversion degree, the MLR method fitted the experimental data to curve shapes based on the different reaction models [45], obtaining the most probable kinetic model of thermal

degradation. The Avrami–Erofeev and n^{th} reaction models were used (Eqs. 12 and 13). Calculations were performed for several reaction schemes, taking into consideration the formal kinetic reaction model: A-1 $\rightarrow$ B-2 $\rightarrow$ C coded as d:f; (consecutive reactions) and A-1 $\rightarrow$ B-2 $\rightarrow$ C-3 $\rightarrow$ D coded as t:f,f; (consecutive reactions) which show that thermal degradation occurs through successive processes in two and three steps. The choice of the optimal model was made on the basis of the criteria presented above and are shown in Table S2 (See Supporting Information). The activation energies for the first stage of degradation depend on the chemical structure of epoxy oil and have a value of 302 kJ mol^{-1} for DGEBA/EFO/RAMA sample and of 323 kJ mol^{-1} for DGEBA/EHO/RAMA sample, while the log A/s^{-1} factor has similar values for both samples, around 20.

Fig. 7_revised

Table 2

Using the data from Table S2 the TG curves were recalculated. Good overlapping of experimental and calculated data curves may be observed (Fig. 7a).

In the case of WECs, the thermal characterization was obtained with same software. Fig. 8a presents the TG and DTA curves of W/DGEBA/EHO/RAMA sample obtained at three heating rates in nitrogen atmosphere. From Fig. 8a, the main degradation parameters ($T_{onset,}$ T_{peak}, T_{10}, T_{20}, T_{50} and W) are extracted and shown in Table 3. Compared with pure polymers, mass losses begin to become significant after 250 ^{o}C. The variation of the apparent activation energy and pre–exponential factor obtained with Friedman method is presented in Fig. 8b. From this figure, the variation of the activation energy of the thermal degradation versus the conversion function degree deviates from linearity, indicating that the thermal degradation process takes place in more than two stages. Using the MLR method with An and n^{th} equations, the most probable kinetic model for A-1 $\rightarrow$ B-2 $\rightarrow$ C type, coded as d:f; (consecutive reactions) was obtained . The optimal model version for W/DGEBA/EFO/RAMA sample is encoded as d:f; An, Fn, and for W/DGEBA/EHO/RAMA sample encoded as d:f; An, An. The kinetic and statistical parameters obtained for the above models are shown in Table S3 (See Supporting Information). The simulated TG curves obtained based on the data from Table S3, presented in Fig. 8a, are in a good agreement with experimental data, suggesting that the theoretical models accurately approximate the experimental data. For the sample W/DGEBA/EFO/RAMA, in Table S3 in the second degradation step, the reaction order has a value greater than 1, suggesting that oligomers are generated during the thermal degradation process [55].

Table 3

Fig. 8_revised

3.6. Chemical composition of the evolved gases

In Scheme 3 there is presented the probable mechanism of thermal degradation of the W/DGEBA/EFO/RAMA cured sample. The gaseous products which appear as result of thermal degradation were identified using FT–IR analysis. In Fig. 9a it is shown the 3D FT–IR spectrum and in Fig. 9b the 2D FT–IR spectrum, extracted at the maximum temperature in the Gram Schmidt plot (365 ^{o}C) of the evolved gases which appear during thermal degradation of the W/DGEBA/EFO/RAMA cured sample, registered at 10 ^{o}C min^{-1}. From the 2D FT–IR spectra (Fig. 9b) it is observed a relatively large number of signals located at 3735 cm^{-1}, 3649 cm^{-1}, 3568 cm^{-1}, 3257 cm^{-1} , 2937 cm^{-1} , 2360 cm^{-1}, 1740 cm^{-1}, 1508 cm^{-1}, 1261 cm^{-1},1177 cm^{-1}, 827 cm^{-1}, 669 cm^{-1} and 538 cm^{-1}. The identification of the signals was made based on literature data [28]. Thus, the signals situated between 3750 and 3500 cm^{-1} can be attributed to OH groups from water vapors or alcohols which resulted from the thermal degradation of the ester and secondary hydroxyl groups. On the other hand, the signal located at 3257 cm^{-1} can be assigned to secondary alcohols and phenols which resulted from degradation of lignin and epoxy resin moieties [56]. The signals assigned to CH, CH_2 and CH_3 groups specific to aliphatic and aromatic hydrocarbon residues are located between 3101 cm^{-1} and 2800 cm^{-1}, as well as 1652 cm^{-1} and 1461 cm^{-1}. These groups result from oil and DGEBA moieties degradation. The strong signal from 2360 cm^{-1} can be attributed to carbon dioxide from the degradation of ester groups. Hemicelluloses and cellulose from wood are mainly composed of D–glucopyranose rings, linked together by 1–4–glycosidic bonds. By cleaving these linkages, D–glucopyranose rings appear which, by recombination, lead to levoglucosan formation. With temperature rise and in the presence of water levoglucosan is transformed into carboxylic derivatives. The signals between 1860 to 1650 cm^{-1} with a maximum located at 1740 cm^{-1} can be attributed to acids, ketones, aldehydes and esters moieties, resulted from the degradation of wood, RAMA and oil. The signals between 1650 cm^{-1} and 1500 cm^{-1} corroborate with the signal situated at 3014 cm^{-1} and can be assigned to aromatic rings from benzene, toluene, phenol, α–methyl styrene, substances that originate from the degradation of DGEBA, RAMA and lignin moieties. The signals situated at 1261 and 1177 cm^{-1} can be assigned to ether C–O–C group.

Scheme 3

Fig. 9_revised

3.7. Resistance to fungi

After 10 weeks of exposure to fungi, both the untreated and the polymer treated samples are covered with fungi colonies, more the blank sample and lesser the polymer coated sample (Fig. 10). After washing and conditioning, the untreated wood sample loses up to 19.4 wt. % depending on the type of fungus, while for the polymer coated wood samples, their weight loss is no more than 2 wt. % (Table 4). It can be seen that the strongest attack is due to *A. brasiliensis* and *C. cladosporioides* for the untreated samples. The polymer covered samples were more attacked by *A. brasiliensis* and *P. chrysogenum*. In the case of pure polymers, all fungi developed very small surface colonies, suggesting that by depositing a thicker layer of polymer may generate an important wood protection effect. Also, in Table 4 there are presented the humidity values after 10 weeks of incubation to fungi exposure. It can be seen that the amount of water absorbed depends on the type of polymer and fungus, the smallest amount being absorbed by W/DGEBA/EHO/RAMA.

Fig. 10_revised

Table 4

3.8. WAXD characterization

Figure 11 shows the WAXD curves of the blank and covered samples registered before and after the fungi decay tests. In general, for pure cellulose, four crystalline peaks ($101, 10\bar{1}$, 002 and 040) have been identified [57]. In our case, the major diffraction peak specific to the crystalline cellulose is located in the range 22.2 – 22.45^{o}, while the diffraction peak specific for the amorphous phases is situated between 18.6 and 18.8^{o} [58, 59]. The fungi preferentially attack the amorphous regions of cellulose, since these regions are less crosslinked in comparison to the crystalline region [60, 61]. These regions may also be highlighted by X–ray analysis. From Table 5 one may observe that the crystallinity index decreases as a result of fungi attack, the lower values being encountered for the unprotected wood samples in comparison with protected samples. This may be due to the blocking by the polymer film of the fungi access to wood.

Fig. 11_revised

Table 5

3.9. SEM and EDAX measurements

As an exemplification, the SEM images obtained in radial section with 1 mm thickness for wood and W/DGEBA/EFO/RAMA sample, decayed in the presence of *C. cladosporioides*, *P. chrysogenum* and *A. brasiliensis* are presented in Figure 12. From these images, it can be seen that the raw wood sample masses have developed a large number of fungus hives inside, while the samples protected with DGEBA/EFO/RAMA were not affected. The results are in good agreement with literature data [62]. Using the EDAX analysis it was possible to evaluate the changes in the elemental chemical composition of the surface for raw wood and treated samples after biological decay. Table 6 shows the chemical composition of the sample surfaces for wood and the coated samples. It can be noted that for all the samples there is a significant increase in the percentage of nitrogen as a result of fungal growth. Also, an increase in the percentage of oxygen for the unprotected samples can be observed, which may be due to the appearance of some carboxyl derivatives occurred during cellulose biodegradation. In the case of wood, there appears a significant decrease in the carbon percentage due to the consumption of wood components. The decrease of microelements content may be attributed to the mass increase of the organic product due to the coating process.

Fig. 12

Table 6

Conclusions

New wood composite materials based on synthetic and natural epoxy derivatives have been obtained and tested in terms of the influence on the thermal stability and fungi resistance. The wood composites were obtained by immersion of the wood samples in a solution of DGEBA/EO/RAMA in acetone and thermally cured. The kinetic parameters of the curing reaction of DGEBA/EO/RAMA and the thermal characterization of crosslinked DGEBA/EO/RAMA and WECs were obtained using DSC and TG methods. The most probable mechanisms of the curing and thermal degradation processes occurred in two or three steps. The decay resistance of wood, DGEBA/EO/RAMA polymers and WECs was obtained by exposure to three fungi (*A. brasiliensis*, *P. chrysogenum* and *C. cladosporioides*) and evaluated with the aid of WAXD and SEM/EDAX methods. Under fungi action, the crystallinity index decreased, the largest drop being registered under the attack of *A. brasiliensis*. Also, the mass loss was higher after the attack of *A. brasiliensis*, reaching 19.4 wt. % for wood, while for the WECs this loss was only 2 wt. %. The polymer

coatings blocked the access of the fungi in the sample masses, thus inducing a superior resistance to their attack.

Acknowledgments

This work was supported by a grant of the Romanian National Authority for Scientific Research and Innovation, CCCDI–UEFISCDI project number ERANET–ERA IB 2–ProWood, within PNCDI III.

Authors are grateful to Dr. Nita Tudorachi, Chem. Elena Marlica and Ph.D. student Daniela Rusu of the ”Petru Poni” Institute of Macromolecular Chemistry in Iasi, Romania, for the evolved gases, FT–IR and SEM/EDAX measuremets.

Conflict of interest

The authors declare no conflict of interest.

References

1. Pandey KK, Pitman A. Examination of the lignin content in softwood and a hardwood decayed by a brown-rot fungus with the acetyl bromide method and Fourier transform infrared spectroscopy. J Polym Sci Part A: Polym Chem 2004;42:2340–2346.

2. Chang ST, Hon DNS, Feist WC. Photodegradation and photoprotection of wood surfaces. Wood Fiber 1982;14:104–117.

3. Norimoto M. Chemical modification of wood. In: Hon DNS, Shiraishi N, editors. Wood and Cellulosic Chemistry. New York: Marcel Dekker, 2001. p. 573–598.

4. Bodîrlău R, Teacă C–A, Rosu D, Rosu L, Varganici C–D, Coroaba A. Physico–chemical properties investigation of softwood surface after treatment with organic anhydride. Cent Eur J Chem 2013;11:2098–2106.

5. Chang HT, Chang ST. Modification of wood with isopropyl glycidyl ether and its effects on decay resistance and light stability. Bioresour Technol 2006;97:1265–1271.

6. Devi R, Maji T. Effect of nanofillers on flame retardancy, chemical resistance, antibacterial properties and biodegradation of wood/styrene acrylonitrile co–polymer composites. Wood Sci Technol 2013;47:1135–1152.

7. Srimalanon P, Yamsaengsung W, Kositchaiyong A, Wimolmala E, Isarangkura K, Sombatsompop N. Effects of UV–accelerated weathering and natural weathering conditions on anti–fungal efficacy of wood/PVC composites doped with propylene glycol–based HPQM. eXPRESS Polym Lett 2016:10;289–301.

8. Li Y, Liu Z, Dong X, Fu Y, Liu Y. Comparison of decay resistance of wood and wood–polymer composite prepared by in–situ polymerization of monomers. Int Biodeterior Biodegrad 2013;84:401–406.

9. Rosu L, Varganici C–D, Mustata F, Rusu T, Rosu D, Rosca I, Tudorachi N, Teacă C–A. Enhancing the thermal and fungal resistance of wood treated with natural and synthetic derived epoxy resins. ACS Sustain Chem Eng 2018;6:5470−5478.

10. Li Y, Dong X, Liu Y, Li J, Wang F. Improvement of decay resistance of wood via combination treatment on wood cell wall: swell–bonding with maleic anhydride and graft copolymerization with glycidyl methacrylate and methyl methacrylate. Int Biodeterior Biodegrad 2011;65:1087–1094.

11. Hazarika A, Mandal M, Maji TK. Dynamic mechanical analysis, biodegradability and thermal stability of wood polymer nanocomposites. Compos Part B: Eng 2014;60:568–576.

12. Candelier K, Thevenon M–F, Petrissans A, Dumarcay S, Gerardin P, Petrissans M. Control of wood thermal treatment and its effects on decay resistance: a review. Ann For Sci 2016;73(3):571–583.

13. Xie Y, Wang Z, Huang Q, Zhang D. Antifungal activity of several essential oils and major components against wood–rot fungi. Ind Crops Prod 2017;108:278–285.

14. Guner FS, Yagci Y, Erciyes AT. Polymers from triglyceride oils. Prog Polym Sci 2006;31:633–670.

15. Xia Y, Larock RC. Vegetable oil–based polymeric materials: synthesis, properties, and applications. Green Chem 2010;12:1893–1909.

16. Rosu D, Mustata F, Tudorachi N, Musteata E, Rosu L, Varganici C–D. Novel bio–based flexible epoxy resin from diglycidyl ether of bisphenol A cured with castor oil maleate. RSC Adv 2015;5:45679–45687.

17. Pin J–M, Sbirrazzuoli N, Mija A. From epoxidized linseed oil to bioresin: An overall approach of epoxy/anhydride cross–linking. ChemSusChem 2015;8:1232–1243.

18. Tan SG, Chow WS. Thermal properties, curing characteristics and water absorption of soybean oil–based thermoset. eXPRESS Polym Lett 2011;5(6):480–492.

19. Hirayama K–I, Irie T, Teramoto N, Shibata M. High–performance bio–based thermosetting resins composed of dehydrated castor oil and bismaleimide. J Appl Polym Sci 2009;114:1033–1039.

20. Rosu D, Mustata F, Tudorachi N, Varganici C–D, Rosu L, Musteata VE. A study on coating properties of an epoxy system hardened with maleinized castor oil. Prog Org Coat 2016;99:480–489.

21. Manthey NW, Cardona F, Francucci G, Aravinthan T. Thermo–mechanical properties of acrylated epoxidized hemp oil based biocomposites. J Comp Mater 48;2014:1611–1622.

22. Mustata F, Tudorachi N. Thermosets based on castor oil modified with Diels–Alder adduct of levopimaric acid and diglycidyl ether of bisphenol A. The kinetic analysis of the curing reactions and thermal behavior of the cured products. Compos Part B: Eng 2016;97:263–273.

23. Mustata F, Tudorachi N, Bicu I. Curing kinetics, thermal and morphological characterization of the biobased thermosets from epoxy resin/epoxidized hemp oil. J Anal Appl Pyrol 2016;122:191–201.

24. Rosu D, Bodîrlău R, Teacă C–A, Rosu L, Varganici C–D. Epoxy and succinic anhydride functionalized soybean oil for wood protection against UV light action. J Clean Prod 2016;112:1175–1183.

25. Roudsari GM, Mohanty AK, Misra M. Study of the curing kinetics of epoxy resins with biobased hardener and epoxidized soybean oil. ACS Sustain Chem Eng 2014;2:2111–2116.

26. Jebrane M, Cai S, Sandström C, Terziev N. The reactivity of linseed and soybean oil with different epoxidation degree towards vinyl acetate and impact of the resulting copolymer on the wood durability. eXPRESS Polym Lett 2017;11:383–395.

27. Temiz A, Kose G, Panov D, Terziev N, Alma MH, Palanti S, Akbas S. Effect of bio–oil and epoxidized linseed oil on physical, mechanical, and biological properties of treated wood. J Appl Polym Sci 2013;130:1562–1569.

28. Mustata FR, Tudorachi N, Bicu I. Biobased epoxy matrix from diglycidyl ether of bisphenol A and epoxidized corn oil, cross–linked with Diels−Alder adduct of levopimaric acid with acrylic acid. Ind Eng Chem Res 2013;52:17099−17110.

29. Atta AM, Mansour R, Abdou MI, El–Sayed A–M. Synthesis and characterization of tetra–functional epoxy resins from rosin. J Polym Res 2005;12:127–138.

30. Liu XQ, Huang W, Jiang YH, Zhu J, Zhang CZ. Preparation of a bio–based epoxy with comparable properties to those of petroleum–based counterparts. eXPRESS Polym Lett 2012;6(4):293–298.

31. Bicu I, Mustata F. Water soluble polymers from Diels–Alder adducts of abietic acid as paper additives. Macromol Mater Eng 2000;280– 281(7–8):47–53.

32. Wang HH, Liu B, Liu XQ, Zhang JW, Xian M. Synthesis of biobased epoxy and curing agents using rosin and the study of cure reactions. Green Chem 2008;10:1190–1196.

33. Bicu I, Mustata F. Study of the condensation products of abietic acid with formaldehyde at high–temperatures. Angew Makromol Chem 1994;222(1);165–174.

34. Mantzaridis C, Brocas AL, Llevot A, Cendejas G, Auvergne R, Caillol S, Carlotti S, Cramail, H, Rosin acid oligomers as precursors of DGEBA–free epoxy resins. Green Chem 2013;15(11):3091–3098.

35. Mustata F, Bicu I. Polyhydroxyimides from resinic acids. Polimery 2000;45:258–263.

36. May CA. Epoxy Resins Chemistry and Technology. New York: Marcel Dekker, 1988.

37. Pascault JP, Williams RJJ. Epoxy Polymers. Weinheim: Wiley–VCH Verlag GmbH & Co. KGaA, 2010.

38. Czub P. A Comparison of the syntheses of high molar mass epoxy resins on the basis of two groups of modified vegetable Oils. Macromol Symp 2009;277:162–170.

39. Czub P. Synthesis of high–molecular–weight epoxy resins from modified natural oils and Bisphenol A or Bisphenol A–based epoxy resins. Polym Adv Technol 2009;20:194–208.

40. Mustata F, Tudorachi N. Epoxy resins crosslinked with rosin adduct derivatives. Crosslinking and thermal behaviors. Ind Eng Chem Res 2010;49:12414–12422.

41. D465–05, Standard Test Methods for Acid Number of Naval Stores Products Including Tall Oil and Other Related Products.

42. D1652– 0, Standard Test Method for Epoxy Content of Epoxy Resins.

43. Mendez ANF, Gregorio JR, da Rosa RG. Studies on the experimental variables effects on rhodium catalyzed hydroformylation of unsaturated fatty esters and comparison of $[RhH(CO)(PPh_3)_3]$ and $[RhCl_3.3H_2O]$ as starting catalytic precursors. J Braz Chem Soc 2005;16(6A):1124–1129.

44. Vyazovkin S, Chrissafis K, Di Lorenzo ML, Koga N, Pijolat M, Roduit B, Sbirrazzuoli N, Suñol JJ. ICTAC Kinetics Committee recommendations for collecting experimental thermal analysis data for kinetic computations. Thermochim Acta 2014;590:1–23.

45. Opfermann J. Kinetic analysis using multivariate non–linear regression. I. Basic Concepts. J Therm Anal Calorim 2000;60:641–658.

46. Flynn HJ, Wall LA. General treatment of the thermogravimetry of polymers. J Res Nat Bur Stand A Phys Chem 70;1966:487–523.

47. Ozawa T. A modified method for kinetic analysis of thermoanalytical data. J Therm Anal 1976;9:369–373.

48. Friedman HL. Kinetic of thermal degradation of char forming plastics from thermogravimetry–application of phenolic plastics. J Polym Sci 1965;C–6:183–195.

49. Worzakowska M. The kinetic study of the curing reaction of mono- and di–epoxides obtained during the reaction of divinylbenzene and hydrogen peroxide with acid anhydrides. Polymer 2007;48:1148–1154.

50. Edelmann M, Gedan–Smolka M, Heinrich G, Lehmann D. Thermokinetic analysis of two–step curing reactions in melt Part I. Investigation of low molecular model systems. Thermochim Acta 2007;452:59–64.

51. Mwaikambo LY, Ansell MP. Chemical modification of hemp, sisal, and kapok fibers by alkalization. J. Appl. Polym. Sci. 2002;84:2222–2234.

52. Popescu CM, Larsson PT, Vasile C. Carbon–13 CP/MAS solid state NMR and X–ray diffraction spectroscopy studies on lime wood decayed by Chaetomium globosum. Carbohydr Polym 2011;83:808–812.

53. Cascaval CN, Ciobanu C, Rosu D, Rosu L. Polyurethane–epoxy maleate of bisphenol A semi-interpenetrating polymer networks. J Appl Polym Sci 2002;83:138–144.

54. Sperling LH. Introduction to Physical Polymer Science. New Jersey: Wiley–Interscience, John Willey & Sons, 2006.

55. Rosu D, Rosu L, Brebu M. Thermal stability of silver sulfathiazole–epoxy resin network. J Anal Appl Pyrol 2011;92:10–18.

56. Worzakowska M, Scigalski P. Synthesis and thermal behavior of linear neryl diesters in inert and oxidative atmosphere. J Therm Anal Calorim 2014;115:783–793.

57. Park S, Baker JO, Himmel ME, Parilla PA, Johnson DK. Celluose crystallinity index: measurement techniques and their impact on interpreting cellulase performance. Biotechnol Biofuels 2010;3:10.

58. Ouajai S, Hodzic A, Shanks RA. Morphological and grafting modification of natural cellulose fibers. J Appl Polym Sci 2004;94:2456–2465.

59. Bari E, Mohebby B, Naji HR, Oladi R, Yilgor N, Nazarnezhad N, Ohno KM, Nicholas DD. Monitoring the cell wall characteristics of degraded beech wood by white–rot fungi: anatomical, chemical, and photochemical study. Maderas–Cien Tecnol 2018;20:35–56.

60. Illman BL. Oxidative degradation of wood by brown–rot fungi. In: Pell E, Steffen K, editors. Active oxygen/oxidative stress and plant metabolism. Philadelphia: American Society of Plant Physiologists, 1991.

61. Lykidis C, Bak M, Mantanis G, Németh R. Biological resistance of pine wood treated with nano–sized zinc oxide and zinc borate against brown–rot fungi. Eur J Wood Prod 2016;74:909–911.

62. Tamburini D, Łucejko JJ, Pizzo B, Mohammed MY, Sloggett R, Colombini MP. A critical evaluation of the degradation state of dry archaeological wood from Egypt by SEM, ATR–FTIR, wet chemical analysis and Py(HMDS)–GC–MS. Polym Degrad Stab 2017;146:140–54.

Schemes and Figures captions

Scheme 1. The synthesis of epoxy oil.

Fig.1. Variation of the swelling coefficient with the solubility parameter for: (●) DGEBA/EFO/RAMA and (○) DGEBA/EHO/RAMA.

Scheme 2. The possible mechanism of the thermal curing of the DGEBA/EO/RAMA sample.

Fig.2. FT–IR spectra of flax oil (a) and epoxidized flax oil (b).

Fig.3. ^{1}H–NMR spectra of flax oil (a) and epoxidized flax oil (b).

Fig.4. FT–IR spectra of W (a), crosslinked DGEBA/EFO/RAMA (b) and WEC (c).

Fig.5 DSC curves for DGEBA/EFO/RAMA (a) and DGEBA/EHO/RAMA (b) at: (■) 5 ^{o}C min^{-1}, at (●) 10 ^{o}C min^{-1} and at (▲) 15 ^{o}C min^{-1} (symbols represent experimental data and lines represent simulated data).

Fig.6. Dependence of the (■) activation energy and the (●) pre–exponential factor versus the conversion degree for the curing of: DGEBA/EFO/RAMA (a) and DGEBA/EHO/RAMA (b) calculated with Friedman method.

Fig.7. TG and DTG curves for: DGEBA/EFO/RAMA at: (■) 10 ^{o}C min^{-1}, at (●) 20 ^{o}C min^{-1} and at (▲) 30 ^{o}C min^{-1} (symbols represent experimental data and lines represent simulated data) (a). Dependence of the (■) activation energy and the (●) pre–exponential factor versus the conversion degree for DGEBA/EFO/RAMA calculated with Friedman method (b).

Fig.8. TG and DTG curves for: DGEBA/EHO/RAMA at: (■) 10 ^{o}C min^{-1}, at (●) 20 ^{o}C min^{-1} and at (▲) 30 ^{o}C min^{-1} (symbols represent experimental data and lines represent simulated data) (a). Dependence of the (■) activation energy and the (●) pre–exponential factor versus the conversion degree for DGEBA/EHO/RAMA calculated with Friedman method (b).

Scheme 3. The possible mechanism of the thermal degradation of the cured DGEBA/EO/RAMA sample.

Fig.9. 3D FT–IR and 2D FT–IR spectra, of the evolved gases during thermal degradation of the W/DGEBA/EFO/RAMA cured sample, registered at 10 ^{o}C min^{-1} heating rate.

Fig.10. Blank and the polymer-treated sample exposed to fungi: (a) W, W/DGEBA/EHO/RAMA and DGEBA/EHO/RAMA exposed to *A. brasiliensis;* (b) W, W/DGEBA/EHO/RAMA and DGEBA/EHO/RAMA exposed to *C. cladosporioides*; (c) W, W/DGEBA/EHO/RAMA and DGEBA/EHO/RAMA exposed to *P. chrysogenum*; (d) W, W/DGEBA/EFO/RAMA and DGEBA/EFO/RAMA exposed to *A. brasiliensis* (e) W, W/DGEBA/EFO/RAMA and DGEBA/EFO/RAMA

exposed to *C. cladosporioides*; (f) W, W/DGEBA/EFO/RAMA and DGEBA/EFO/RAMA exposed to *P. chrysogenum*

Fig.11. (a) WAXD curves for: W (1); W decayed with *A. brasiliensis* (2)*;* W decayed with *C. cladosporioides* (3)*;* W decayed with *P. chrysogenum* (4); (b) WAXD curves for: DGEBA/EHO/RAMA decayed with *C. cladosporioides* (1); DGEBA/EHO/RAMA undecayed (2); DGEBA/EHO/RAMA decayed with *A. brasiliensis* (3); and DGEBA/EHO/RAMA decayed with *P. chrysogenum* (4); (c) WAXD curves for: DGEBA/EFO/RAMA decayed with *P. chrysogenum* (1)*;* DGEBA/EFO/RAMA decayed with *C. cladosporioides* (2); DGEBA/EFO/RAMA decayed with *A. brasiliensis* (3) and DGEBA/EFO/RAMA undecayed (4).

Fig.12. SEM micrographs of the cross–section of W decayed with: *C. cladosporioides* (a), *P. chrysogenum* (b) and *A. brasiliensis* (c); W/DGEBA/EFO/RAMA decayed with: *C. cladosporioides* (d), *P. chrysogenum* (e) and *A. brasiliensis* (f).

Table 1. Solvents and their corresponding solubility parameters (δ)

Number	Solvent	δ (cal cm^{-3})$^{0.5}$
1	n-Hexane	7.24
2	Carbon tetrachloride	8.05
3	Cyclohexane	8.18
4	Xilene	8.85
5	Toluene	8.91
6	Ethyl acetate	9.1
7	Chloroform	9.21
8	Tetrahidrofurane	9.52
9	Acetone	9.77
10	Cyclohexanone	9.88
11	Methylene chloride	9.93
12	Dioxane	10
13	Acetic acid	10.1
14	Dimethyl acetamide	11.0
15	Isopropyl alcohol	11.6
16	Dimethyl formamide	12.14
17	Dimethyl sulfoxide	12.93
18	Methanol	14.28
19	Diethylene glycol	14.6
20	Ethylene glycol	16.3
21	Glycerol	21.1
22	Water	23.5

Table 2.
Thermal degradation parameters obtained by TG analysis of cured samples at three heating rates.

Sample	Heating rate	T_{onset}	T_{peak}	W_{600}	T_{10}	T_{20}	T_{50}
	$^{o}C \cdot min^{-1}$	^{o}C	^{o}C	%	^{o}C	^{o}C	^{o}C
DGEBA/EFO/RAMA	10	380	422	1.2	259	374	413
	20	380	427	2.1	325	374	418
	30	378	430	5.2	331	375	425
DGEBA/EHO/RAMA	10	383	419	1.1	339	380	419
	20	383	429	2.2	355	387	429
	30	377	436	5.4	363	390	499

T_{onset} – the temperature at which the thermal degradation start;
T_{peak} – the temperature at which the degradation rate is maximum;
T_{10}, T_{20}, T_{50} - the temperatures corresponding to 10 wt.%, 20 wt.%, 50 wt.% mass losses;
W_{600}- residual mass at 600 ^{o}C

Table 3.
The thermal parameters obtained by TG analysis of cured W/DGEBA/EO/RAMA samples at three heating rates

Sample	Heating rate	T_{onset}	T_{peak}	W_{600}	T_{10}	T_{20}	T_{50}
	$^oC \cdot min^{-1}$	^oC	^oC	%	^oC	^oC	^oC
W/DGEBA/EFO/RAMA	10	319	356	17.4	286	320	361
	20	322	363	27.8	286	326	370
	30	323	365	20.9	285	328	378
W/DGEBA/EHO/RAMA	10	321	354	20.5	296	323	362
	20	329	364	22.9	302	330	380
	30	320	371	20.2	298	330	381

T_{onset} – the temperature at which the thermal degradation starts;
T_{peak} – the temperature at which the degradation rate is maximum;
T_{10}, T_{20}, T_{50} - the temperatures corresponding to 10 wt.%, 20 wt.%, 50 wt.% mass losses;
W_{600} - residual mass at 600 ^oC

Table 4. Some characteristic of the samples, registered after a10 week exposure against *A. brasiliensis*, *P. chrysogenum* and *C. cladosporioides* strains.

Sample	mean weight loss[a] WL (%)			humidity[a,] H (%)		
	A. brasiliensis	*P. chrysogenum*	*C. cladosporioides*	*A. brasiliensis*	*P. chrysogenum*	*C. cladosporioides*
W	19.4	4.47	6.37	50.4	50.5	33.5
W/DGEBA/EHO/RAMA	1.82	1.38	0.43	6.97	22.6	26.7
W/DGEBA/EFO/RAMA	1.89	1.39	1.22	38.5	36.9	16.7

a) Means were for 4 samples

Table 5. Crystalline index

Sample	Undecayed blank	*A. brasiliensis* decayed	*P. chrysogenum* decayed	*C. cladosporioides* decayed
W	74.0	67.58	70.04	70.1
W/DGEBA/EHO/RAMA	67.4	63.2	64.4	64.13
W/DGEBA/EFO/RAMA	69.2	63.6	67.7	67.0

Means were for 4 samples

Table 6. SEM/EDAX composition of wood and W/DGEBA/EO/RAMA samples

Element	Sample									
	W			W/DGEBA/EHO/RAMA			W/DGEBA/EFO/RAMA			
	undecayed	decayed with *C. cladosporioides*	decayed with *P.chrysogenum*	decayed with *A.brasiliensis*	decayed with *C. cladosporioides*	decayed with *P.chrysogenum*	decayed with *A.brasiliensis*	decayed with *C. cladosporioides*	decayed with *P.chrysogenum*	decayed with *A.brasiliensis*
C	66.2	58.42	58.45	55.85	71.68	70.52	71.94	68.65	58.30	69.08
N	1.66	4.60	3.55	4.51	4.62	6.10	5.45	3.77	5.31	4.72
O	30.11	35.23	36.82	36.4	23.63	25.2	21.20	33.22	35.15	32.63
Fe	0.62	0.63	0.30	0.61	0.33	0.39	0.25	0.47	0.23	0.63
Na	0.24	0.23	0.24	0.45	0.10	0.15	0.11	0.16	0.13	0.11
Mg	0.04	0.04	0.05	0.07	0.09	0.06	0.20	0.08	0.10	0.08
Al	0.18	0.11	0.06	0.06	0.08	0.12	0.29	0.11	0.12	0.12
Si	0.25	0.14	0.16	0.21	0.12	0.10	0.11	0.10	0.13	0.11
Cl	0.17	0.15	0.14	0.02	0.18	0.15	0.12	0.09	0.12	0.19
K	0.16	0.20	0.17	0.15	0.17	0.08	0.89	0.07	0.14	0.13
Ca	0.16	0.16	0.13	0.14	0.11	0. 10	0.19	0.15	0.12	0.11

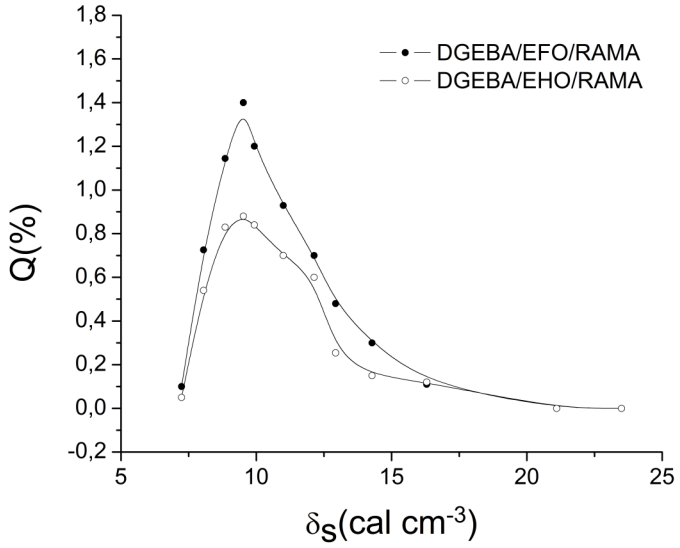

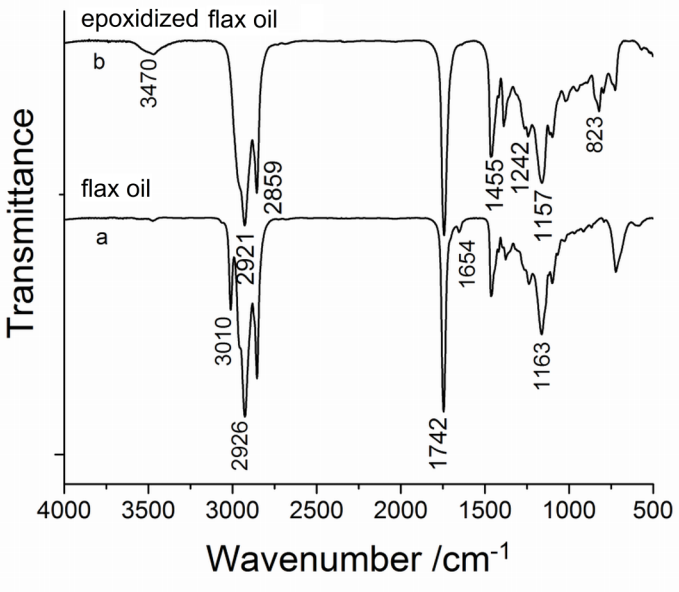

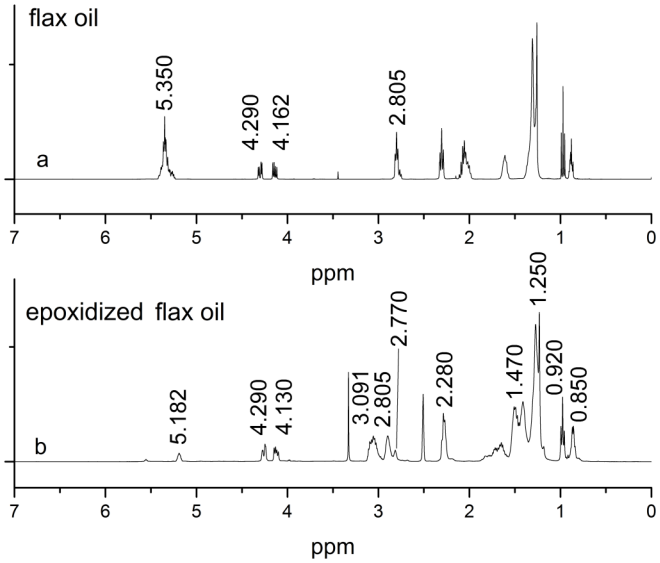

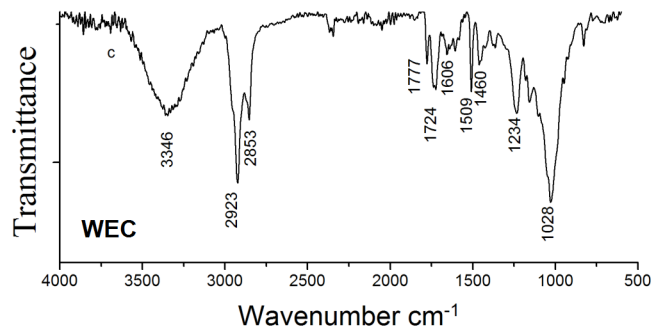

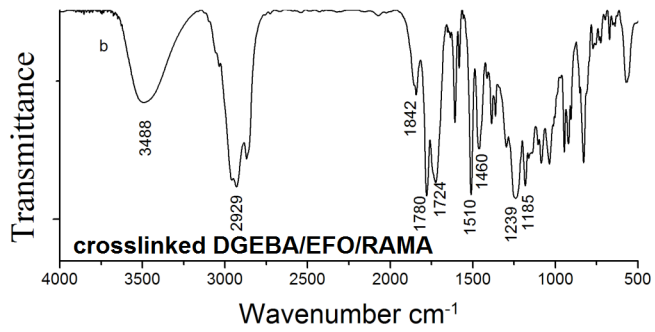

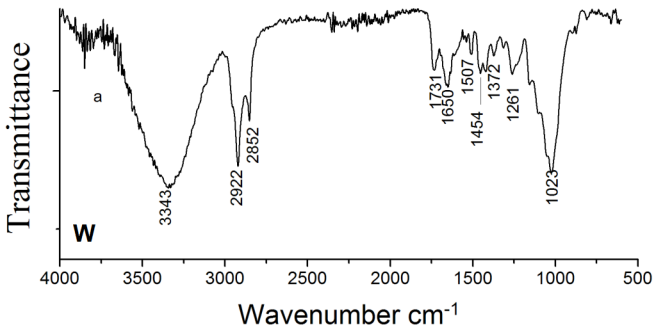

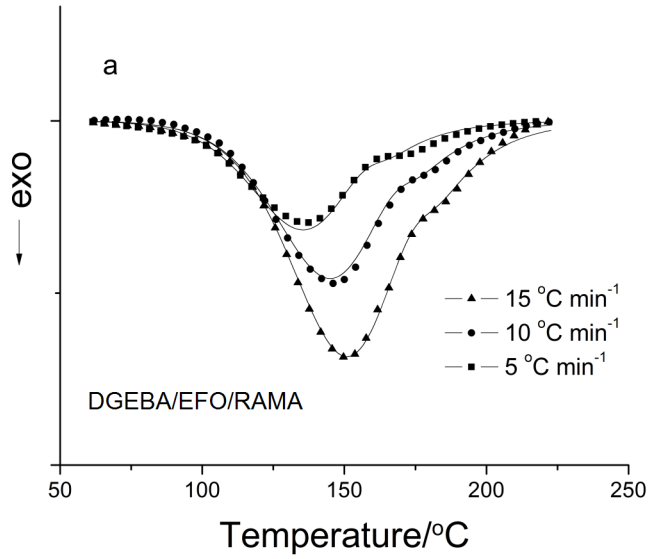

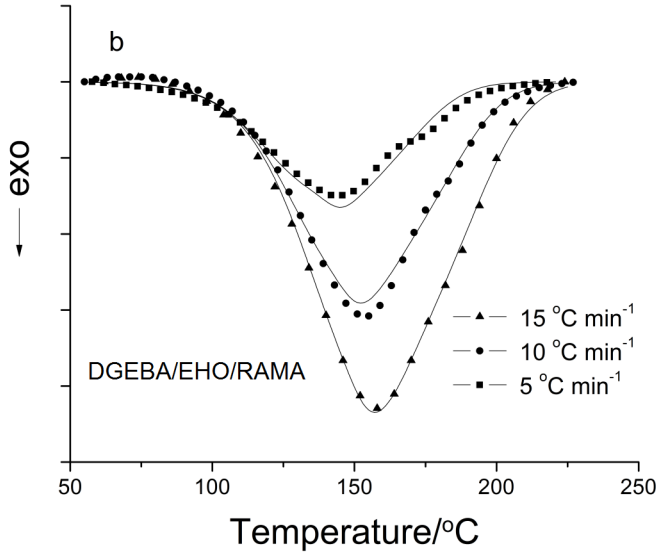

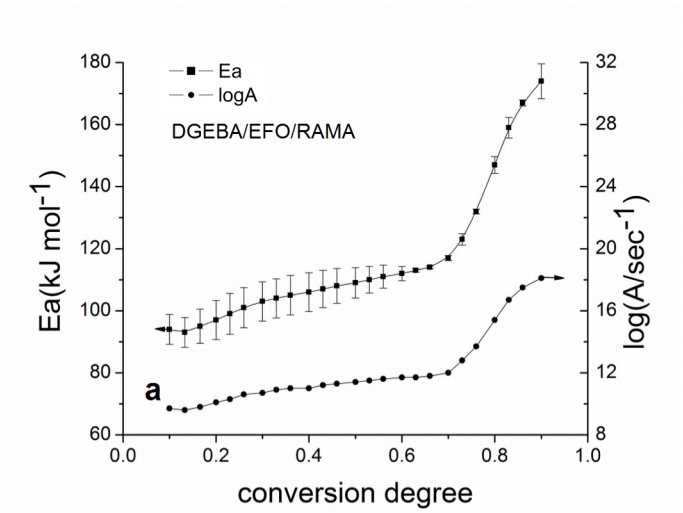

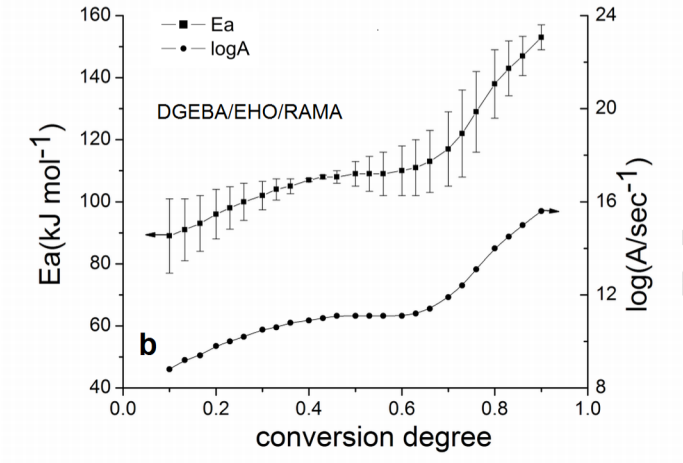

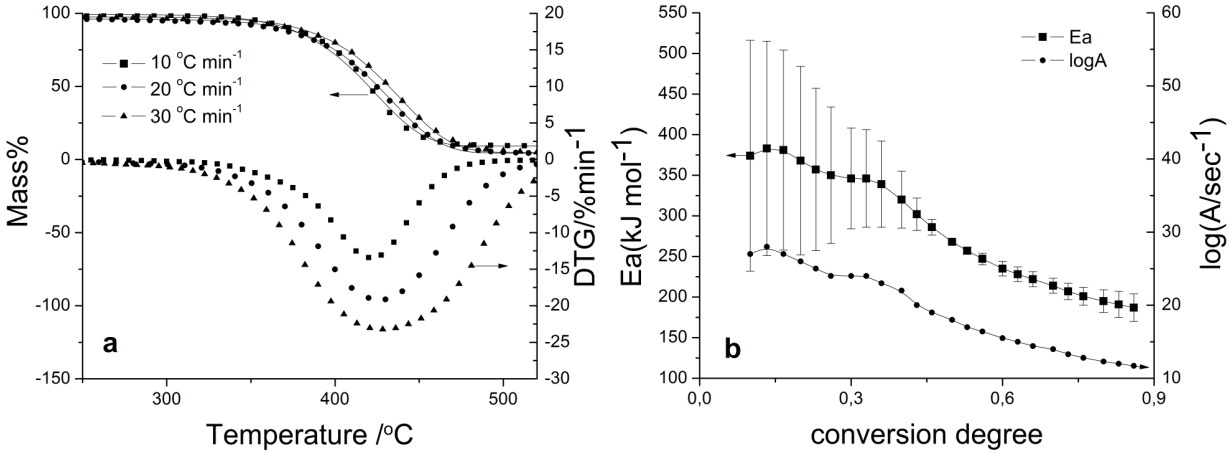

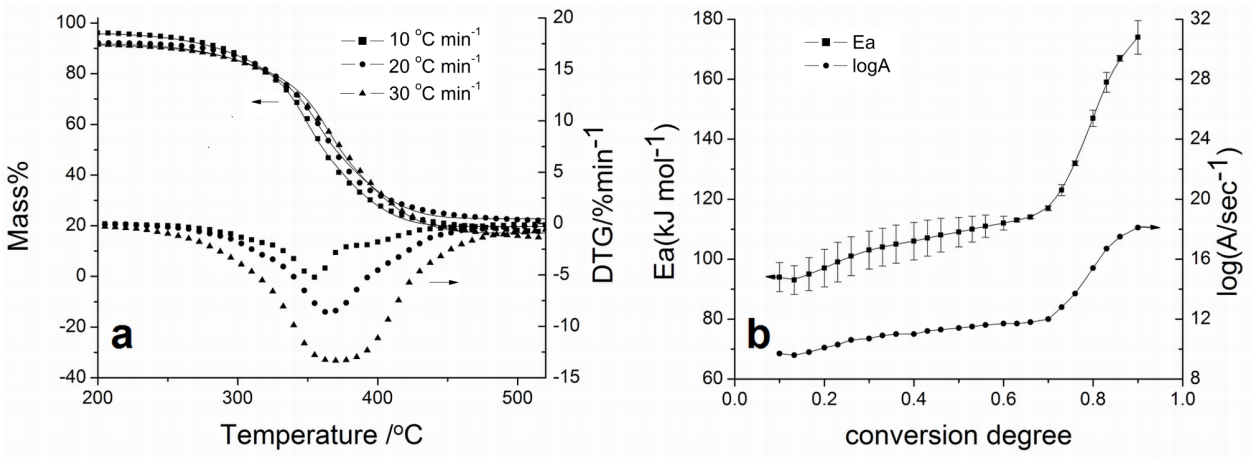

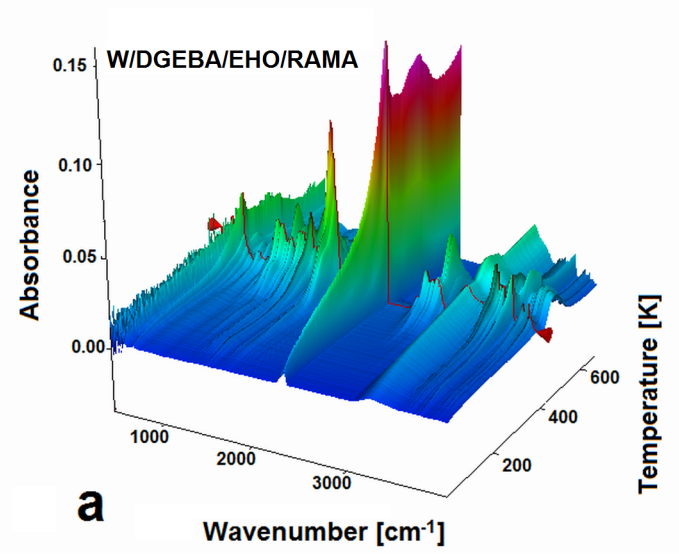

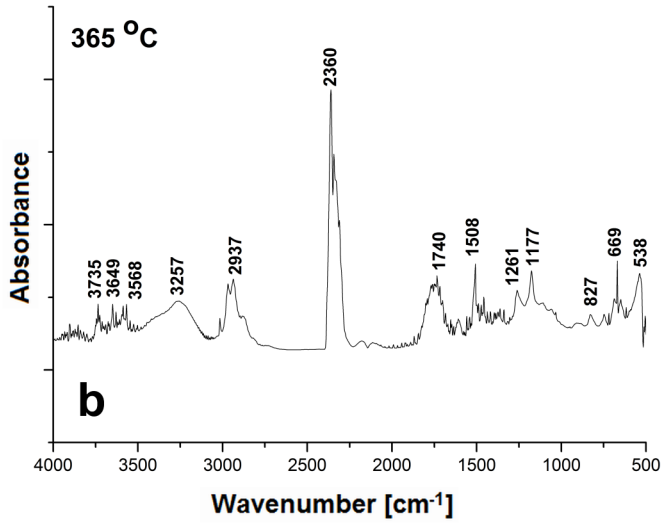

a W, W/DGEBA/EHO/RAMA, DGEBA/EHO/RAMA exposed to *A. brasiliensis*

b W, W/DGEBA/EHO/RAMA, DGEBA/EHO/RAMA exposed to *C. cladosporioides*

c W, W/DGEBA/EHO/RAMA, DGEBA/EHO/RAMA exposed to *P. chrysogenum*

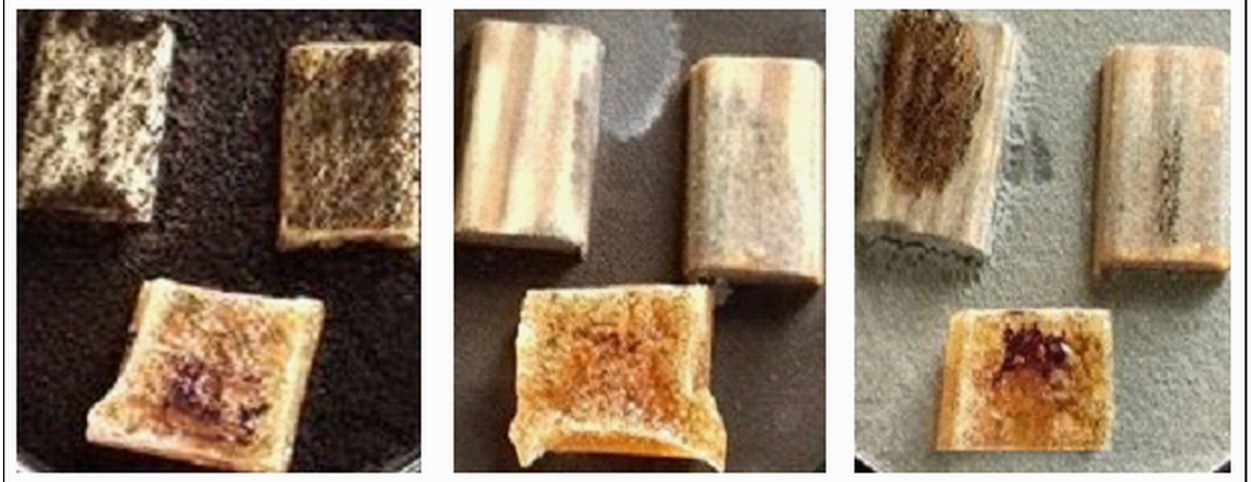

d W, W/DGEBA/EFO/RAMA, DGEBA/EFO/RAMA exposed to *A. brasiliensis*

e W, W/DGEBA/EFO/RAMA, DGEBA/EFO/RAMA exposed to *C. cladosporioides*

f W, W/DGEBA/EFO/RAMA, DGEBA/EFO/RAMA exposed to *P. chrysogenum*

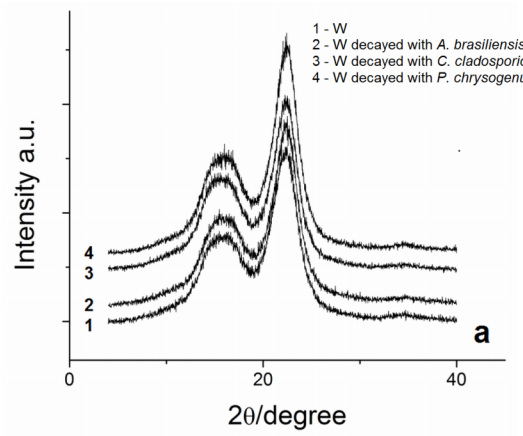
1 - W
2 - W decayed with A. brasiliensis
3 - W decayed with C. cladosporioides
4 - W decayed with P. chrysogenum
Intensity a.u.
4
3
2
1
a
0
20
40
2θ/degree

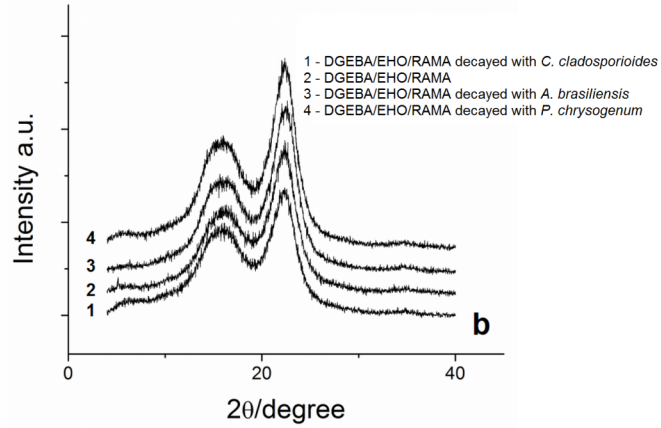
1 - DGEBA/EHO/RAMA decayed with C. cladosporioides
2 - DGEBA/EHO/RAMA
3 - DGEBA/EHO/RAMA decayed with A. brasiliensis
4 - DGEBA/EHO/RAMA decayed with P. chrysogenum
Intensity a.u.
4
3
2
1
b
0
20
40
2θ/degree

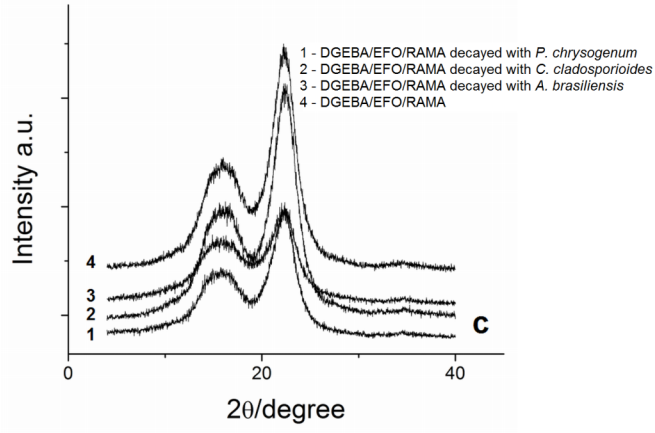
1 - DGEBA/EFO/RAMA decayed with P. chrysogenum
2 - DGEBA/EFO/RAMA decayed with C. cladosporioides
3 - DGEBA/EFO/RAMA decayed with A. brasiliensis
4 - DGEBA/EFO/RAMA
Intensity a.u.
4
3
2
1
c
0
20
40
2θ/degree

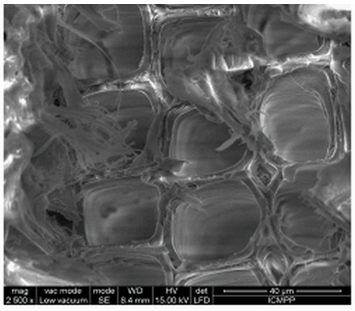

W decayed with Cladosporium cladosporioides (a)

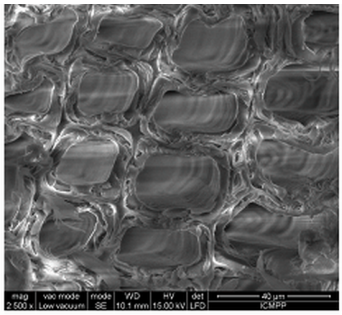

W decayed with Penicilium chrysogenum (b)

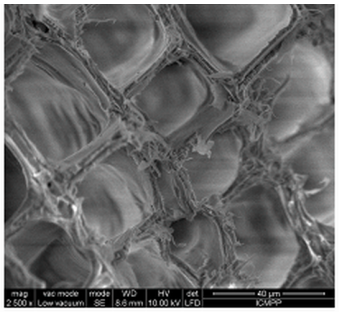

W decayed with Aspergillus brasiliensis (c)

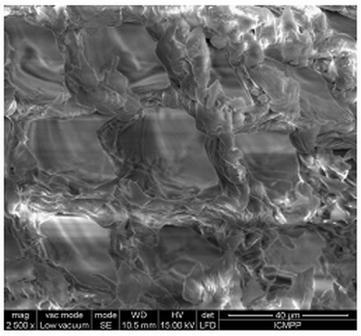

W/DGEBA/EFO/RAMA decayed with Cladosporium cladosporioides (d)

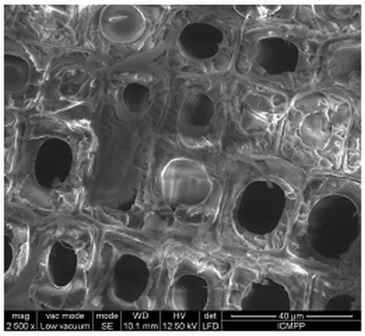

W/DGEBA/EFO/RAMA decayed with Penicilium chrysogenum (e)

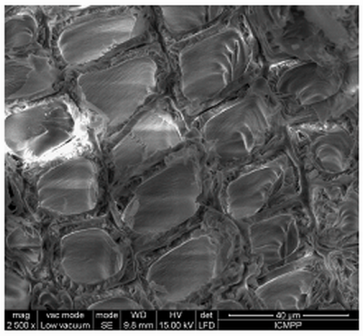

W/DGEBA/EFO/RAMA decayed with Aspergillus brasiliensis (f)

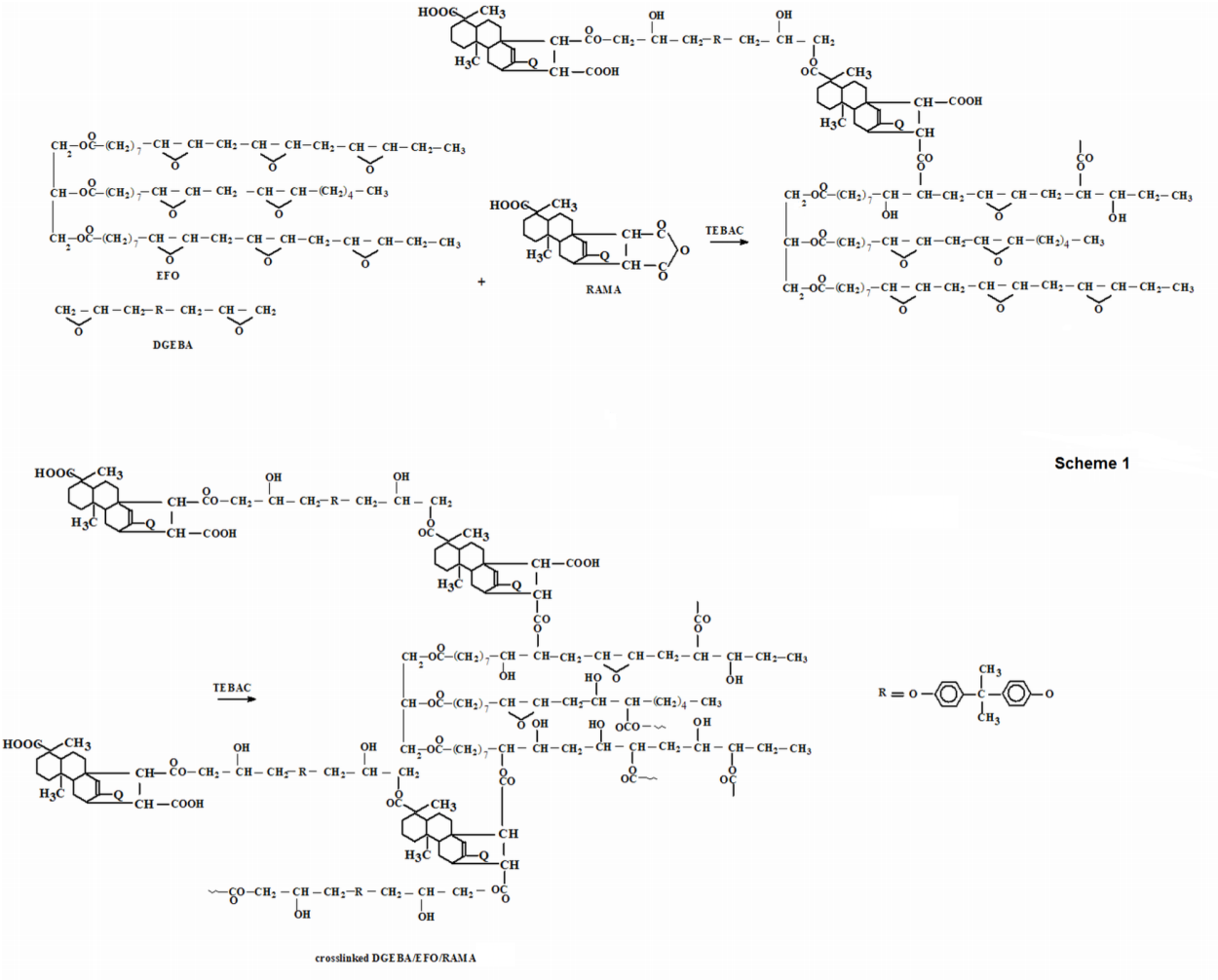

Scheme 1

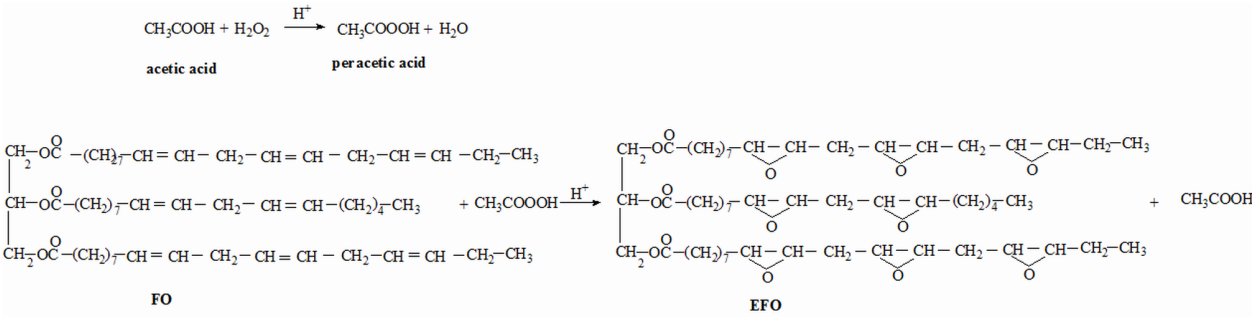

Scheme 2

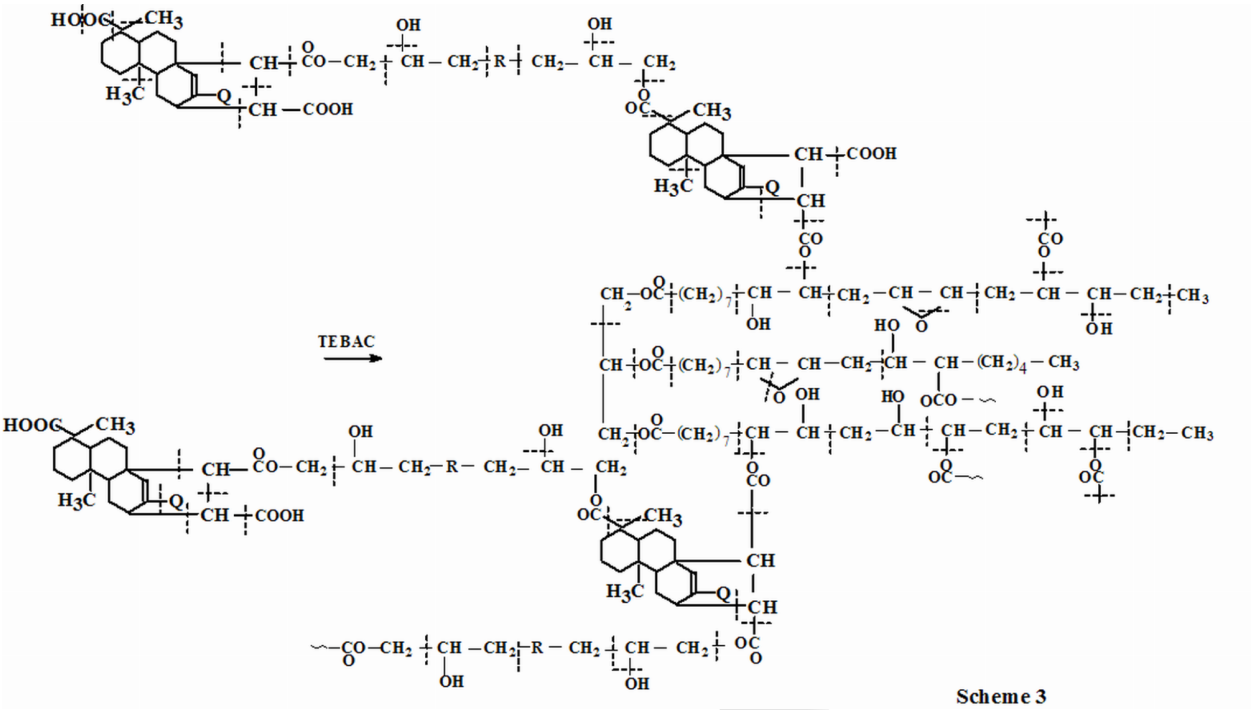

Scheme 3

- New synthetic and natural epoxy derivatives as wood coatings were obtained.
- The epoxy derivatives were thermally crosslinked.
- The influence of coating on wood thermal stability and fungi resistance was made.